

Bipolar Thermoelectricity in Bilayer-Graphene–Superconductor Tunnel Junctions


L. Bernazzani^{1,2,*}, G. Marchegiani³, F. Giazotto⁴, S. Roddaro^{1,4} and A. Braggio^{4,†}

¹*Dipartimento di Fisica “E. Fermi”, Università di Pisa, Pisa I-56127, Italy*

²*Fachbereich Physik, Universität Konstanz, Konstanz D-78457, Germany*

³*Quantum Research Center, Technology Innovation Institute, Abu Dhabi P.O. Box 9639, United Arab Emirates*

⁴*NEST, Istituto di Nanoscienze CNR & Scuola Normale Superiore, Pisa I-56127, Italy*

 (Received 15 July 2022; revised 21 February 2023; accepted 23 February 2023; published 6 April 2023)

We investigate the thermoelectric properties of a hybrid nanodevice composed of a two-dimensional carbon-based material and a superconductor. This system presents nonlinear bipolar thermoelectricity, as induced by the spontaneous breaking of the particle-hole (PH) symmetry in a tunnel junction between bilayer graphene (BLG) and a Bardeen-Cooper-Schrieffer superconductor. In this scheme, the nonlinear thermoelectric effect, predicted and observed in superconductor-insulator-superconductor' junctions, is not affected by the competitive effect of the Josephson coupling. From a fundamental perspective, the most intriguing feature of this effect is its bipolarity. The capability to open and control the BLG gap guarantees improved thermoelectric performances that reach up to 1 mV/K, regarding the Seebeck coefficient, and a power density of 1 nW/ μm^2 for temperature gradients of tens of kelvin. Furthermore, the externally controlled gating can also dope the BLG, which is otherwise intrinsically PH symmetric, giving us the opportunity to investigate the bipolar thermoelectricity, even in the presence of the controlled suppression of the PH symmetry. The predicted robustness of this system could foster further experimental investigations and applications in the near future, thanks to the available nanofabrication techniques.

DOI: [10.1103/PhysRevApplied.19.044017](https://doi.org/10.1103/PhysRevApplied.19.044017)

I. INTRODUCTION

Thermoelectricity is conventionally investigated in materials where there is a well-defined dominant carrier [1–3]. Indeed, the Boltzmann theory of transport demonstrates that in the linear-response regime the Seebeck coefficient has the same sign as the charge of the dominant carrier [1,4]. In other words, thermoelectricity seems to be present only in systems where the particle-hole (PH) symmetry is broken to a certain extent [5]. This becomes paradigmatic in superconducting systems, where it should be expected that PH symmetry and the dissipationless flow of Cooper pairs would implicitly limit any thermoelectric effect. Nevertheless, a few studies [6,7] anticipated that even superconducting systems could exhibit thermoactive behavior. Along this route, theoretical [8–18] and experimental [19–21] research shows that nonlocality or phase coherence may still trigger intriguing thermoelectric phenomena in superconducting and hybrid systems. Furthermore, some authors even reported the existence

of absolute negative conductance (ANC) in superconducting tunnel junctions under out-of-equilibrium conditions or microwave irradiation [22–25].

More recently, instead, in a number of theoretical papers [26–29], the spontaneous breaking of the PH symmetry was predicted in superconductor-insulator-superconductor' (S - I - S') tunnel junctions subject to a finite thermal gradient. In these studies, a strong bipolar thermoelectric effect is clearly identified in the nonlinear regime of the thermal bias. These predictions are confirmed experimentally [30,31], also providing methods to make superconducting nonvolatile memory [26,32] or other spin-active devices [33].

However, there are several drawbacks concerning the physical realization of the cited effect in asymmetric S - I - S' junctions. The most serious issue is given by the Josephson coupling, which needs to be substantially suppressed [30], as theoretically anticipated in Ref. [28]. Indeed, the Josephson effect may completely kill the thermoelectric generation of power by shunting the junction at low biases, i.e., $|eV| \ll (\Delta_R + \Delta_L)$, here $\Delta_{R(L)}$ are the values of the bulk superconducting-gap function on the two sides of the S - I - S' junction, therefore restoring the PH symmetry and suppressing the thermoelectric effect. This limitation may be even more serious under out-of-equilibrium

*Corresponding author: lorenzo.bernazzani@uni-konstanz.de

†<https://sites.google.com/site/alessandrobaggio/Home>

conditions, since the Josephson coupling presents anomalous jumps when thermal gradients are applied to an asymmetric S - I - S' superconducting junction [34,35]. Hence, the possibility of making a junction using a semiconductor coupled to superconductors instead would be beneficial in this respect. Furthermore, this nonlinear thermoelectric effect manifests strongly at the so-called “matching-peak” conditions, $V_{\text{peak}} = \pm|(\Delta_R - \Delta_L)/e|$, where the singularities in the Bardeen-Cooper-Schrieffer (BCS) density of states (DOS) are aligned. So, the possibility to engineer, in detail, the semiconducting gaps would be beneficial for the performance of the device.

Nevertheless, the aforementioned bipolar thermoelectric effect requires that the semiconductors forming the junction have a gap comparable to those of the superconductors to which they are coupled, i.e., they should have gaps of the order of a few meV [36,37]. On the other hand, elemental or binary-compound semiconductors have gaps larger than hundreds of meV [36]. This fact pushes us to consider a completely different platform, i.e., carbon-based low-dimensional materials, that can exhibit smaller band gaps, the values of which can even be tuned, in some cases, by electrostatic gating [38].

Herein, we demonstrate the bipolar thermoelectricity in hybrid junctions composed of bilayer graphene (BLG) coupled to BCS superconductors (S) through an insulating barrier (I). Notably, the band gap of BLG is controllable by electrical gating [39], making it possible to adapt the band gap to the best operating conditions, which are connected to the superconducting gap and the temperature of the hot lead (BLG), by changing just the electric gate voltages. This peculiar phenomenon increases the flexibility and performances of the device. For instance, it allows one to switch thermoelectricity in the junction *on* and *off*. Moreover, the replacement of one of the superconducting electrodes with BLG relaxes the constraints on the hot-electrode temperature, leading to an even wider applicability of the thermoactive elements, which, in principle, can operate up to hundred of kelvins.

II. DEVICE DESCRIPTION

Low-dimensional systems have attracted a lot of interest recently [44], and intriguingly have already been discussed as promising materials for improving the thermoelectric performance in the pioneering work of Ref. [45]. BLG, in particular, is a two-dimensional material formed by two planes of graphene stacked on top of each other. It naturally inherits the intrinsic PH symmetry of graphene if it is not extrinsically doped. However, its bands deviate from the conventional linear-dispersion relationships of graphene [46,47]. In fact, by tight-binding computations [48,49], one can show that they are characterized by a nonlinear-dispersion relationship [50]. Similarly to

monolayer graphene, BLG is a semimetal, and, in the pristine form, valence and conduction bands touch each other at the high-symmetry K , K' points. Notably, by applying an electric field perpendicular to the BLG plane, a gapped phase can be induced, effectively behaving as an electrically controllable semiconductor. In Fig. 1(a), we display a sketch of the setup discussed below, where the BLG is coupled to a top and bottom gate that may be tuned externally. The gate-controlled resultant band gap is highlighted in Fig. 1(b). In the absence of gating, the BLG is gapless and the dispersion of the lowest-energy band is approximately quadratic, $\epsilon(k) = \pm(\sqrt{1 + 4(v_F \hbar k)^2} - 1)/2 \approx \pm(v_F \hbar k)^2$ (orange solid curves) [41], with v_F as the Fermi velocity. BLG's gap can be opened and controlled by applying a differential gating between the back gate, $V_{g,B}$, and the top gate, $V_{g,T}$ [41,42] (solid red curves). However, gating may also induce charge doping at the BLG planes, spoiling the perfect PH symmetry and paving the way to the intriguing possibility of investigating a bipolar thermoelectric device in the presence of a controlled breaking of the PH symmetry as well. As reported in Ref. [42], this tunable band gap can be computed using the following approximate formula [41,42]:

$$2E_g = \frac{|U|t_{\perp}}{\sqrt{U^2 + t_{\perp}^2}}, \quad (1)$$

where U is the potential-energy difference between the two graphene planes, also called the gating asymmetry parameter, and $t_{\perp} \approx 0.4$ eV is the interlayer-hopping-energy term in the tight-binding approximation of BLG's electronic band structure. The approximate energy dispersion in the gapped state [41] $\epsilon(k) \approx \pm\sqrt{U^2/4 + \pm(v_F \hbar k)^4/t_{\perp}^2}$ is shown in Fig. 1(b) (solid red curve).

This paper deals with the theoretical study of a BLG- I - S tunnel junction, the schematic representation of which is given in Fig. 1(a). The BLG is on the left side of the junction and is deposited on the silica substrate. We suppose to be able to heat up the BLG electronic temperature to induce an effective thermal gradient across the junction by means of irradiation by a photon source or by the Joule effect due to normal currents flowing between electrodes [51,52] [this can usually be accomplished using other normal metal electrodes, e.g., yellow contact in Fig. 1(a)]. The BLG is in clean contact with a gold (Au) electrode [see Fig. 1(a)], so that the voltage drop, V , applied across the structure localizes at the BLG- I - S junction. In other words, the Au electrode and the BLG are equipotential. The electrostatic gating is applied with the aid of a top gate, $V_{g,T}$ capacitively coupled to BLG through an oxide and a Si^+ layer, with the role of the bottom gate, beneath the silica layer, as shown in Fig. 1(a) [40,53]. The right electrode composing the junction is a BCS superconductor

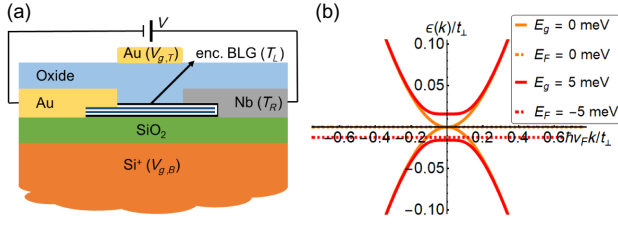


FIG. 1. a) Schematics of the proposed device. BLG is placed on top of a silica (SiO_2) dielectric ($\epsilon_b = 3.9$) 100 nm thick, beneath which there is the bottom gate (doped Si). BLG is encapsulated in a h -BN monolayer but is ohmic coupled with a Au electrode on the left side. Niobium (Nb) superconducting electrode is deposited partially on top of the BLG. h -BN constitutes the tunneling barrier with the superconducting electrode. Finally, an oxide ($\epsilon_t = 7.5$) [40], approximately 190 nm thick, is deposited above the electrodes, and a top gate made from Au is placed on top of this dielectric. (b) Band scheme of the BLG [41–43]. Gap is opened using the top and bottom gates. With the dashed lines, we also show how the BLG Fermi energy, E_F^{BLG} , moves along the bands, due to an asymmetric gating effect. We assume $v_F \approx 10^6$ m/s as the Fermi velocity in graphene.

[gray in Fig. 1(a)]. To have a superconducting gap commensurate with those of BLG and, at the same time, a good range of operating temperatures, we choose Nb for the BCS superconductor. This metal has a critical temperature of $T_c \approx 9$ K. It is deposited partially on the encapsulated BLG to provide a tunnel contact with it. The encapsulation of BLG is made from a monolayer of hexagonal boron nitride (h -BN). This material constitutes proper tunnel barriers, since it is a good insulator with an almost perfect crystallographic order [54].

III. BIPOLAR THERMOELECTRICITY WITH PH SYMMETRY

In the tunneling framework, we can compute the charge and heat currents according to [26,27,37,55,56]

$$\begin{aligned} \begin{bmatrix} I \\ \dot{Q}_L \end{bmatrix} &= \frac{4\pi |T|^2}{\hbar} \int_{-\infty}^{+\infty} d\epsilon \begin{bmatrix} -e \\ \epsilon \end{bmatrix} N_{\text{BLG}}(\epsilon) N_S(\epsilon + eV) \\ &\times [f_L(\epsilon) - f_R(\epsilon + eV)], \end{aligned} \quad (2)$$

where $|T|$ is the transmittivity of the tunneling barrier, which, in our case, is given by the h -BN layer between the BLG and the superconducting electrode. In writing Eq. (2), we further assume that the barrier transmissivity is independent of the gate voltages, $V_{g,T}$ and $V_{g,B}$, applied to the BLG. This approximation is reasonable at the energy scales considered in this work, where the induced BLG band gaps and the applied voltage bias are in the order of a few meV, but may fail for a very strong gating. The electron gas in the semi- and superconductive leads follows the Fermi-Dirac distribution, $f_i(\epsilon, T_i) = [1 + \exp(\epsilon/k_B T_i)]^{-1}$, where we assume that carriers are in quasiequilibrium,

which is well described by a standard quasiparticle distribution with an electronic temperature of T_i [57]. We also introduce the tunneling-barrier bias voltage, V .

In Eq. (2), the DOS of the two electrodes are $N_{\text{BLG}(S)}(E)$. In our case, the right electrode is a BCS superconductor; therefore,

$$N_S(\epsilon) = N_F \left| \text{Re} \left[\frac{\epsilon + i\Gamma_D}{\sqrt{(\epsilon + i\Gamma_D)^2 - \Delta_R(T_R)^2}} \right] \right| \quad (3)$$

where N_F is the DOS of the metal in the normal state at the Fermi energy, $\Delta_R(T_R)$ is the superconducting gap, and Γ_D is the Dynes phenomenological correction to the BCS DOS [58]. On the other hand, the left electrode is composed of the BLG, the DOS of which for $E \ll t$ can be approximated as [41,59]

$$N_{\text{BLG}}(\epsilon) \approx \frac{t_\perp}{\sqrt{3} \pi t^2} \frac{|E| \Theta(|E| - E_g)}{\sqrt{E^2 - E_g^2}}, \quad (4)$$

where $\Theta(x)$ is the Heaviside step function, and $E = \epsilon + E_F^{\text{BLG}}$, with E_F^{BLG} being the BLG's Fermi energy. The tight-binding energies for the in-plane hopping integral of graphene is $t \approx 3$ eV, and the out-of-plane hopping term is $t_\perp \approx 0.4$ eV. We assume that the insulating barrier between BLG and the superconductor (Nb) is formed by h -BN [60]. We also assume a tunneling conductance of $G_T \approx (10 \text{ k}\Omega)^{-1}$ [61] for h -BN separating the BLG electrode, above which the superconducting electrodes will be deposited, forming a junction of about $0.1 \mu\text{m}^2$; this choice is consistent with values reported in Ref. [62]. Despite a larger active surface leading to a higher conductance, which would be beneficial for the performance of the proposed junction, it is nonetheless important that the barrier between the leads is a good insulating barrier, since we are going to establish a sizeable temperature gradient across the junction. Furthermore, enlargement of the active surface could also lead to unwanted effects, such as pinhole points [63].

Clearly, either asymmetric gating or charge traps at the oxide surface may also induce a deviation in the midgap position of the BLG's Fermi energy, E_F^{BLG} , partially breaking the PH symmetry. However, with two independent top and bottom gates, it is always possible to restore the PH symmetry in the BLG. Indeed, since the band gap, $2E_g \approx U$ [for $U \ll t_\perp$, see Eq. (1)], is induced mainly by the differential gating mode, the common mode can be exploited to modify E_F^{BLG} , changing the BLG doping [40–42,48,64,65]. More specifically, we can find a line of points in the $(V_{g,B}, V_{g,T})$ plane for which the BLG turns out to be fully PH symmetric and gapped. This is a straight line with a slope of $-C_b/C_t$, where $C_i = \epsilon_0 \epsilon_i / d_i$ are the capacitances with top ($i = t$) or bottom ($i = b$) gates determined by the thicknesses, $d_b(d_t)$, of the oxide layers and their

dielectric constant, ϵ_t (ϵ_b) [40]. We note that the charge accumulated in the BLG through gating modifies the Fermi energy, and thus, the total junction differential conductance (see discussion in Sec. III). However, these effects cannot be interpreted as a gating dependence of the transmissivity of the tunneling barrier. Therefore, in the first part of this paper, we investigate the device under gating conditions where the BLG electrode is fully PH symmetric, i.e., $E_F^{\text{BLG}} = 0$, according to our notation. In this configuration, due to the PH-symmetric nature of the electrodes, one should expect that the junction can never display linear thermoelectric behavior [5,66]. Nevertheless, when BLG's electronic temperature and thermal gradients exceed finite thresholds, we predict the possibility of inducing spontaneously a thermoelectric regime in the junction just by tuning BLG's gap at values higher than Nb's superconducting gap. Furthermore, it is easy to check that the PH symmetry of the two leads, i.e., $N_i(E) = N_i(-E)$, will result in the antisymmetric nature of the current with respect to the electric bias, i.e., $I(V) = -I(-V)$. This phenomenology is similar to that reported in Refs. [26,27,30]. However, it is worth noting that the possibility of tuning the electrode gap through gating, is unique to this system. In fact, in the S - I - S' case, one should change the material composing the electrode [30] or induce complex phase-controlled gaps in proximity junctions [35].

The discussed bipolar thermoelectric effect is nonlinear, since a finite-temperature difference is required to activate the junction. When $E_g > \Delta_R(T_R)$, the junction can be in the thermoactive regime, i.e., displaying ANC $IV < 0$, for an appropriate temperature difference between the two terminals. In Fig. 2, we show the I - V characteristics in the subgap regime when the junction is thermoactive. The electronic temperature of the BLG is assumed to remain a high temperature [e.g., $T_L = 50$ K in Fig. 2(a)] and the superconductor will be on the cold side with $T_R = T_{\text{bath}} = 1$ K [67]. Similarly to the S - I - S' case [27], we can identify two different thermoelectric regimes that depend exclusively on the absolute module, $|V|$. These are the linear-in-bias regime, which is revealed by the negative differential conductance at $V \approx 0$, and the nonlinear-in-bias effect, which manifests strongly with the biggest ANC at the matching-peak condition, $|eV_p| = E_g(U) - \Delta_R(T_{\text{bath}})$. By looking at the peaks in Figs. 2(a) and 2(b), we observe how their position is changed following the evolution of the BLG gap, E_g , which is modified by external gating. Notably, we see that the height of the ANC peaks is weakly dependent on the BLG gap [see Fig. 2(a)] but is more affected by the temperature of BLG [see Fig. 2(b)]. Finally, we note that, in this configuration, where the BLG is hot and the superconductor is cold, the hot temperature does not affect the position of the peak, since E_g depends only on the electrostatic potential, U . This is a substantial difference with respect to the S - I - S' case [26,27,30]. As a consequence, it is also important that the thermoelectric

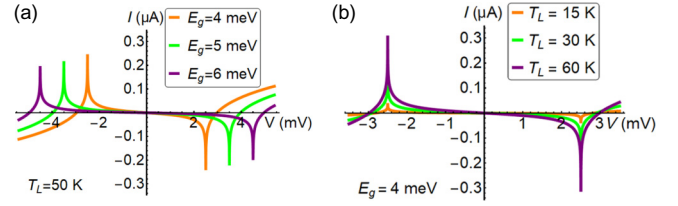


FIG. 2. I - V characteristics of the proposed junction in the thermoelectric regime, $E_g > \Delta_R(T_R)$. Thermoelectricity is easily spotted because $IV < 0$, and this implies ANC. (a) I - V characteristics plotted by varying BLG's gap (obtained by varying the gating voltages, while keeping the BLG in the PH-symmetry line). Here, the BLG temperature is kept at $T_L = 50$ K. (b) I - V characteristics plotted by varying the electronic temperature of BLG while keeping the BLG gap fixed at $2E_g = 8$ meV. Height of the peak, and consequently, strength of thermoelectricity, grows by increasing the hot-lead temperature. Peculiarly, due to the nonlinearity of the effect, it appears that the Seebeck voltage, V_S , defined by $I(V_S) = 0$, depends weakly on the BLG temperature being more connected to the position of the matching peak, V_p , instead, which, in this system, is unaffected by T_L . In the computation, we assume that the superconductor resides at a bath temperature of $T_R = T_{\text{bath}} = 1$ K, a Dynes parameter of $\Gamma_D/\Delta = 10^{-4}$, and a tunneling conductance of $G_T = (10 \text{ k}\Omega)^{-1}$.

power, $P = -IV$, is a monotonously increasing function of the hot temperature in our system, in contrast to the S - I - S' concept, where closing of the gap with temperature limits the thermoelectricity to a well-defined range, spanning, at most, an interval of a few kelvin.

Since we are not dealing with a linear thermoelectric effect, we cannot rely on standard figures of merit typical for thermoelectric elements, such as ZT [5,68]. Hereafter, we focus on alternative figures of merit to quantify the performances of the BLG- I - S thermoelectric junction in comparison with other recent proposals [30]. In particular, it is interesting to show them, as in Fig. 3, by using contour plots. Therefore, investigating how they depend on both the BLG gap, E_g , and temperature, T_L . In Fig. 3(a), we show the maximum thermocurrent, $I_{\text{max}} = |I(\pm V_p)|$, which is obtained at the matching-peak voltage, V_p , and, correspondingly, in Fig. 3(b), the thermoelectric power delivered at the same point, $P(V_p) = -I(V_p)V_p$, by the junction [69]. The gray areas in the plots denote the regions with $E_g < \Delta_R(T_R)$, where the system is purely dissipative, thus producing no net thermoelectric current. Both of the quantities are monotonically increasing functions of BLG temperature, T_L , and quickly saturate for $T_L \gtrsim E_g/k_B$ (not shown). These figures of merit do not behave monotonically with respect to the BLG gap, E_g , displaying a maximum for a temperature-dependent optimal value. We notice that the values of the thermoelectric charge current are quite high for a junction of $0.1 \mu\text{m}^2$. At the same time, the output power, shown in Fig. 3(b), is notably high, since it reaches values above 750 pW for high-temperature

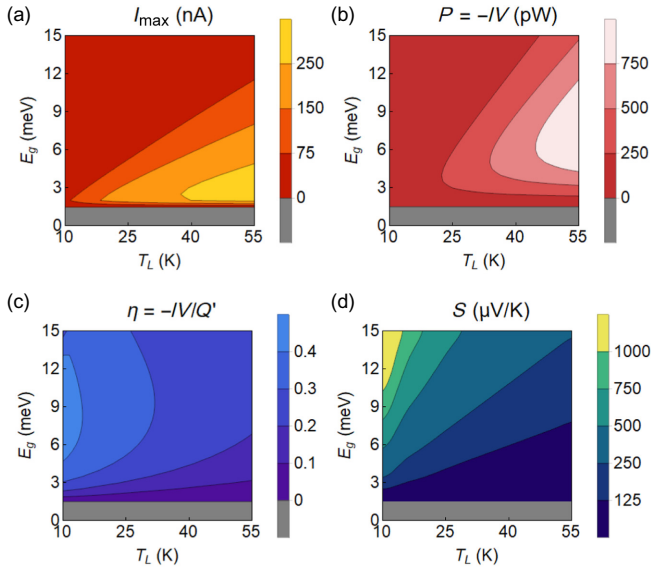


FIG. 3. Thermoelectric figures of merits for the proposed junction at the PH-symmetric point as a function of the BLG band gap, $2E_g$, and the BLG electronic temperature, T_L . (a) Maximum current in nA obtained at the matching-peak condition, $I(V_p)$. (b) Thermoelectric power at the matching peak, $-I(V_p)V_p$, in units of pW. (c) Thermodynamic absolute efficiency computed at the matching peak, V_p , where the output power is roughly maximum. (d) Nonlinear Seebeck coefficient in units of $\mu\text{V/K}$. Remaining parameters are the same as those in Fig. 2.

gradients and intermediate gap values, which correspond to a power density of roughly $1 \text{ nW}/\mu\text{m}^2$. Since it is computed at the matching peak, it is natural to ask how this quantity would be affected by the quality of the superconducting contact, leading to a higher Dynes parameter. We report, without showing it, that the output power of the junctions is only reduced by a logarithmic correction of about a factor of 2 when changing the Dynes parameter by 2 orders of magnitudes (from $10^{-4}\Delta_0$ used here to $10^{-2}\Delta_0$).

Furthermore, it is interesting to discuss, looking at Fig. 3(c), the absolute efficiency of the thermoelectric engine at maximum power. A useful approximation for such a quantity is the value it assumes at $V = V_p$, i.e., $\eta_p \approx -I(V_p)V_p/\dot{Q}_L(V_p)$, since the junction delivers maximum power approximately at the matching-peak point. At the same time, the heat losses in the junction are probably dominated by the quasiparticle contribution, $\dot{Q}_L(V_p)$, computed using Eq. (2) [70]. In this case, the best efficiencies are obtained at the lowest BLG temperatures, T_L , where the decrease in heat losses is much bigger than the decrease of the thermopower. Notably, the absolute efficiency reaches values up to 40% and, when the hot temperature is fixed, there is an optimal value for the gap. It is worth noting that the efficiency here is the absolute thermodynamic efficiency of the thermodynamic machine.

Finally, in Fig. 3(d), the thermoelectric performance is shown in terms of the nonlinear Seebeck coefficient (NSC), which is computed as [26]

$$S = \frac{V_S}{T_L - T_R}, \quad (5)$$

where V_S is computed numerically by finding the point at which the I - V characteristic crosses the zero-current axis, i.e., $I(V_S) = 0$. This is a natural extension, in a nonlinear picture, of the Seebeck coefficient, defined as $S = \lim_{\Delta T \rightarrow 0} \Delta V / \Delta T|_{I=0}$. By the way, this is the solution of the linear thermoelectricity equation: $I = G \Delta V - G S \Delta T = 0$ [5]. This quantity can be computed only in the region where the junction is thermoelectric ($IV < 0$), while the dissipative regions are colored in gray. The values of the NSC demonstrate the strength of thermoelectricity generation in this junction, which reaches values higher than $1000 \mu\text{V/K}$ at the lowest-temperature gradient explored of approximately 9 K. This graph also reveals quite general behavior of this quantity, which increases with the BLG band gap. Looking at Fig. 3(d), we can say that the highest values of the NSC can be reached at low values of temperature gradient, where the thermopower is quite low [see Fig. 3(b)], confirming once again, even in this nonlinear situation, a sort of trade-off between efficiency and power production.

IV. PARTIAL BREAKING OF PH SYMMETRY

Having discussed the PH-symmetric case in Sec. III, we now consider the more general case, where the BLG is not perfectly gated at the PH-symmetric line, i.e., the aforementioned perfect charge-neutrality line of the gates. The loss of PH symmetry on the BLG side, with the stated conventions, can be seen as the case where the Fermi energy is $E_F^{\text{BLG}} \neq 0$. Indeed, according to the self-consistent model of screening, adapted from Refs. [41,42,71], the electrostatic asymmetry parameter, U [and so, the band gap, see Eq. (1)], and the BLG Fermi energy should be computed self-consistently from the value of the electrostatic gating voltages. We state here only the final formula, which can be derived from the more general treatments of Refs. [42,71,72].

A recent experiment [72] shows the important role of localized states, in particular, for designs with silicon dioxide substrate. These localized states contribute to the charge density of the BLG but not to the screening of the electrostatic asymmetry parameter, U [73]. The fundamental parameters needed in the I - V characteristics are the electrostatic asymmetry parameter, U , and the Fermi energy, E_F^{BLG} , which are given by [74]

$$U \approx \frac{e(C_b V_{g,B} - C_t V_{g,T})}{2C_{\text{BLG}}[1 - \ln(|U|/4t_\perp)/2]}, \quad (6)$$

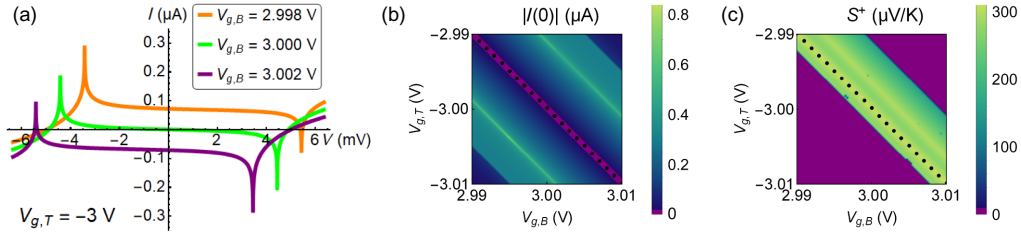


FIG. 4. (a) I - V characteristics for the PH-asymmetric state of BLG (orange and violet lines) for $T_L = 50$ K and $V_{g,T} = -3$ V. Green line is the PH-symmetric case. We notice that these characteristics show thermoelectric behavior, since in the neighborhoods of the peaks $P = -IV > 0$. (b) Current at zero bias (conventional thermocurrent) for $T_L = 50$ K. Purple areas denote regions where $I(0) \approx 0$, a necessary condition for PH symmetry. (c) NSC S^+ for $T_L = 20$ K. Within purple regions, the junction is not thermoelectric and the NSC cannot be defined. $T_R = 1$ K, $\varepsilon_b = 3.9$, $\varepsilon_t = 7.5$, $d_b = 100$ nm, $d_t = 192$ nm, $d = 0.35$ nm.

$$E_F^{\text{BLG}} \approx e \frac{C_b V_{g,B} + C_t V_{g,T}}{C_b + C_t}, \quad (7)$$

where $C_{\text{BLG}} = \varepsilon_0 \varepsilon_r / d$ is the BLG interlayer capacitance, with $d \approx 0.35$ nm as the distance between the two graphene layers and $\varepsilon_r \sim 1$ [75]. The solution of the first equation has to be found numerically for every gate configuration, $(V_{g,B}, V_{g,T})$. The experimental realization of the device determines the gate capacitances, C_i , with $i = t, b$. To simplify the gating around the PH-symmetric point, it is convenient to consider experimental setups where $C_b \approx C_t$. In principle, by plugging these quantities into Eqs. (1) and (4), one can easily determine the BLG gap and the BLG DOS.

In this situation of partial breaking of the PH symmetry, a conventional thermoelectric effect adds to the nonlinear contribution that we outline in Sec. III. However, as we discuss below, this conventional contribution does not completely spoil the bipolar thermoelectricity phenomenology. This result shows that the bipolar thermoelectric effect is also stable against slight perturbations of the PH symmetry of the electrodes. The stability is evident by looking at Fig. 4(a), where we fix $V_{g,T} = -3$ V and slightly change the bottom voltage, $V_{g,B}$, moving around the PH-symmetry point (green line). In this graph, in fact, we see that the current at the matching peak of the I - V characteristics is still thermoelectric ($IV < 0$), even if there is a slight departure from PH symmetry, as signaled by a finite linear thermocurrent contribution, i.e., $I(V=0) \neq 0$. The I - V characteristics, in this case, are no longer reciprocal, i.e., $I(V) \neq -I(-V)$, and they do not cross the origin of the axes. Nevertheless, we notice that the system still displays behavior connected to the spontaneous breaking of PH symmetry. Indeed, at $V = 0$, the differential conductance, dI/dV , is negative for both the orange (violet) line cases. This negative conductance determines an electrical instability. When the system is thermoelectric, $IV < 0$, this device effectively operates as a battery, when connecting the resistive load in parallel, and the junction is able to support two opposite signs for the thermocurrent

through the load for the *same* thermal gradient. In fact, if the load resistance is sufficiently high, we can find two different solutions for the current circulating in the load (just imposing current conservation in the circuit, as in Ref. [27]) with opposite sign. This feature demonstrates that the thermoelectric effect is still bipolar, i.e., two opposite signs of thermocurrent for a given thermal gradient are possible [30]. The intrinsic instability at $V \approx 0$ and the bipolar nature of the effect are consequences of the spontaneous breaking of PH symmetry and would be important in applications such as current-controlled thermoelectrical memory [30,32] or even sensors [76].

It is interesting to investigate how the zero-bias thermoelectric current, $I(0)$, behaves, fixing a finite-temperature gradient, as a function of the voltage of the top and bottom gates, i.e., in the $(V_{g,B}, V_{g,T})$ plane. In Fig. 4(b), we see that this quantity is zero at the PH-symmetry line (purple region). The bright-yellow lines parallel to that are the lines at which the BLG gap equals the superconductor gap, and so, the matching peak is more or less at $V \approx 0$. This interpretation explains why $I(0)$ at these yellow lines is so enhanced. Indeed, we notice that the $I(0)$ current can be quite high and even become comparable to the maximal thermocurrent generated by the bipolar thermoelectric effect discussed before. This thermocurrent can be interpreted as that from a conventional thermoelectric effect but also presenting strong nonlinear enhancement. In other words, we are discussing thermoelectric behavior that is linear in the bias, V , but nonlinear in the thermal gradient.

Clearly, when the PH symmetry is broken, the I - V characteristics are no longer antisymmetric and the bias values, V_S^\pm , for which $I(V_S^\pm) = 0$ are different, depending on the sign of V , i.e., $|V_S^+| \neq |V_S^-|$. As a consequence, we need to define a NSC that is different, depending on the positive (negative) voltage branch, such that $S^\pm = V_S^\pm / (T_L - T_R)$. Considering the NSC S^+ , for instance, we see that it is zero, except for the green-yellow band in Fig. 4(c). The displayed behavior can be understood as follows. In the region of interest, $V_{g,B} \approx -V_{g,T} \approx 3$ V, the band gap is approximately constant, reading $E_g \approx U/2 \approx 6$ meV,

as determined by the self-consistent solution of Eq. (6). Hence, the overall behavior of S^+ is mainly determined by the evolution of the Fermi energy [see Eq. (7)], which varies significantly once away from the PH-symmetry line (black dotted line in Fig. 4). This feature makes the green-yellow band asymmetric with respect to the PH-symmetry line. When considering S^+ , we compute the zero-current state with $V > 0$. For $|V_{g,B}| < |V_{g,T}|$, the current-voltage characteristic shifts towards higher-current values [cf. Fig. 4(a)], which means the thermoelectric peak does not intersect the $I = 0$ axes above a threshold value of E_F^{BLG} . Differently, for $|V_{g,B}| > |V_{g,T}|$, the characteristic is shifted in the opposite direction, and the intersection persists until the matching-peak condition is at $V = 0$. Since the value of the NSC mainly depends on E_g , as discussed above, we notice that, within the green and yellow region, S^+ depends only weakly on the gates (evolution determined by variation of the Fermi energy). The maximum NSC reaches $300 \mu\text{V/K}$ for $T_L = 20 \text{ K}$, in agreement with Fig. 3(d). Finally, we observe that these figures show that small deviations from PH symmetry would not completely spoil the bipolar nonlinear thermoelectric effect, although one clearly loses the full antisymmetry of the I - V characteristics. This fact confirms the robustness of the discussed bipolar thermoelectric effect, since it is stable against small deviations from ideal gating conditions.

V. CONCLUSIONS

Here, we analyze the nonlinear thermoelectricity of a BLG-superconductor tunneling junction. We demonstrate that by external gating it is possible to tune the BLG gap and the thermoelectric effect by only electrical means, achieving very promising values for the figures of merit, e.g., NSC of up to 1 mV/K at a temperature of the BLG of $T_L = 10 \text{ K}$. For such temperature gradients, we predict a thermoelectric generation of power of hundreds of pW for $0.1 \mu\text{m}^2$ of active surface, which corresponds to a surface power density of roughly $1 \text{ nW}/\mu\text{m}^2$, with a maximal absolute thermodynamic efficiency of up to 40% for the electronic degrees of freedom. Finally, we investigate how the different figures of merit depend on the BLG electronic temperature and on the BLG gap in a realistic range of variations of external parameters. The stated bipolar thermoelectric phenomenology could even survive a partial breaking of the PH symmetry, as might be potentially induced by a nonideal external electrostatic gating of the BLG electrode. We discuss, for this more general case as well, the thermoelectric properties of the device, showing, indeed, that there is an interplay between the nonlinear bipolar thermoelectricity induced by spontaneous breaking of the PH symmetry and the conventional unipolar thermoelectricity, as determined by a small PH-breaking term. However, we confirm that this latter contribution can coexist with the former, without being detrimental to the bipolar

thermoelectricity. We state one more time that the phenomenology outlined here could lead to a wide versatility of this sort of device due to the tunability provided by the external-gating mechanism.

Finally, we hope that the sizable thermoelectric performances of this hybrid device architecture, combined with its electrical flexibility, will trigger the future experimental exploration of bipolar thermoelectricity at even higher temperatures. Indeed, the tunability of the gap makes the device adaptable to respond to unwanted changes in the temperature of the hot lead and, at the same time, can be exploited to switch its thermoelectric behavior *on* and *off*. We see that hybrid superconducting-graphene devices can play an important role in calorimetry and fast bolometry [51,77–79]. We can envision similar applications for our device [76]. Furthermore, one can also exploit our system in thermoelectric nanodevices similar to those designed in different platforms [80–83], with the advantage of higher operating temperatures. To conclude, we hope that the peculiar features of the bipolar thermoelectric effect reported here will spur further applications in the field of quantum technologies [32].

ACKNOWLEDGMENTS

The authors wish to thank Dr. A. Tomadin, Dr. T. Novotny, Dr. K. Michaeli, and Professor F. Strocchi for useful discussions. F.G. and A.B. acknowledge the EU's Horizon 2020 research and innovation program under Grant Agreements No. 800923 (SUPERTED) and No. 964398 (SUPERGATE) for partial financial support. S.R. acknowledges financial support from the Italian Ministry of University and Research (PRIN project QUANTUM2D). A.B. acknowledges the Royal Society through International Exchanges between the UK and Italy (Grants No. IEC R2 192166 and No. IEC R2 212041).

-
- [1] T. M. Tritt, *Thermal Conductivity: Theory, Properties, and Applications* (Kluwer Academic/Plenum Publishers, New York, 2004).
 - [2] T. M. Tritt and M. A. Subramanian, Thermoelectric materials, phenomena, and applications: A bird's eye view, *MRS Bull.* **31**, 188 (2006).
 - [3] E. Macià-Barber, *Thermoelectric Materials: Advances and Applications* (Pan Stanford Publishing, Taylor and Francis Group, 2015).
 - [4] G. Grosso and G. P. Parravicini, *Solid State Physics* (Academic Press, Elsevier Ltd., Oxford, 2014), 2nd ed.
 - [5] G. Benenti, G. Casati, K. Saito, and R. Whitney, Fundamental aspects of steady-state conversion of heat to work at the nanoscale, *Phys. Rep.* **694**, 1 (2017).
 - [6] V. Ginzburg, Thermoelectric effects in the superconducting state, *Sov. Phys. Usp.* **34**, 101 (1991).

- [7] A. D. Smith, M. Tinkham, and W. J. Skocpol, New thermoelectric effect in tunnel junctions, *Phys. Rev. B* **22**, 4346 (1980).
- [8] P. Machon, M. Eschrig, and W. Belzig, Nonlocal Thermoelectric Effects and Nonlocal Onsager Relations in a Three-Terminal Proximity-Coupled Superconductor-Ferromagnet Device, *Phys. Rev. Lett.* **110**, 047002 (2013).
- [9] A. Ozaeta, P. Virtanen, F. S. Bergeret, and T. T. Heikkilä, Predicted Very Large Thermoelectric Effect in Ferromagnet-Superconductor Junctions in the Presence of a Spin-Splitting Magnetic Field, *Phys. Rev. Lett.* **112**, 057001 (2014).
- [10] R. Sánchez, P. Burset, and A. L. Yeyati, Cooling by Cooper pair splitting, *Phys. Rev. B* **98**, 241414 (2018).
- [11] S. M. Tabatabaei, D. Sánchez, A. L. Yeyati, and R. Sánchez, Nonlocal quantum heat engines made of hybrid superconducting devices, *Phys. Rev. B* **106**, 115419 (2022).
- [12] S. S. Pershoguba and L. I. Glazman, Thermopower and thermal conductance of a superconducting quantum point contact, *Phys. Rev. B* **99**, 134514 (2019).
- [13] P. Virtanen and T. Heikkilä, Thermopower in Andreev interferometers, *J. Low Temp. Phys.* **136**, 625 (2004).
- [14] P. Jacquod and R. Whitney, Coherent thermoelectric effects in mesoscopic Andreev interferometers, *Europhys. Lett.* **91**, 67009 (2010).
- [15] M. S. Kalenkov and A. D. Zaikin, Large thermoelectric effect in ballistic Andreev interferometers, *Phys. Rev. B* **95**, 024518 (2017).
- [16] R. Hussein, M. Governale, S. Kohler, W. Belzig, F. Giazotto, and A. Braggio, Nonlocal thermoelectricity in a Cooper-pair splitter, *Phys. Rev. B* **99**, 075429 (2019).
- [17] N. S. Kirsanov, Z. B. Tan, D. S. Golubev, P. J. Hakonen, and G. B. Lesovik, Heat switch and thermoelectric effects based on Cooper-pair splitting and elastic cotunneling, *Phys. Rev. B* **99**, 115127 (2019).
- [18] A. Ratnakar and S. Das, Enhancement in tunneling density of states in a Luttinger liquid: Role of nonlocal interaction, *Phys. Rev. B* **104**, 045402 (2021).
- [19] J. Eom, C.-J. Chien, and V. Chandrasekhar, Phase Dependent Thermopower in Andreev Interferometers, *Phys. Rev. Lett.* **81**, 437 (1998).
- [20] Z. Jiang and V. Chandrasekhar, Quantitative measurements of the thermal resistance of Andreev interferometers, *Phys. Rev. B* **72**, 020502 (2005).
- [21] Z. Tan, A. L. N. Kirsanov, A. Galda, V. Vinokur, M. Haque, A. Savin, D. Golubev, G. Lesovik, and P. Hakonen, Thermoelectric current in a graphene Cooper pair splitter., *Nat. Commun.* **12**, 138 (2021).
- [22] A. G. Aronov and B. Z. Spivak, Photoeffect in a Josephson junction, *JETP Lett.* **22**, 101 (1975).
- [23] M. E. Gershenson and M. I. Falei, Absolute negative resistance of a tunnel contact between superconductors with a nonequilibrium quasiparticle distribution function, *JETP Lett.* **44**, 682 (1986).
- [24] M. E. Gershenson and M. I. Falei, Absolute negative resistance in tunnel junctions of nonequilibrium superconductors, *Sov. Phys. JETP* **67**, 389 (1988).
- [25] J. G. Gijsbertsen and J. Flokstra, Quasiparticle injection-detection experiments in niobium, *J. Appl. Phys.* **80**, 3923 (1996).
- [26] G. Marchegiani, A. Braggio, and F. Giazotto, Nonlinear Thermoelectricity with Electron-Hole Symmetric Systems, *Phys. Rev. Lett.* **124**, 106801 (2020).
- [27] G. Marchegiani, A. Braggio, and F. Giazotto, Superconducting nonlinear thermoelectric heat engine, *Phys. Rev. B* **101**, 214509 (2020).
- [28] G. Marchegiani, A. Braggio, and F. Giazotto, Phase-tunable thermoelectricity in a Josephson junction, *Phys. Rev. Res.* **2**, 043091 (2020).
- [29] G. Marchegiani, A. Braggio, and F. Giazotto, Noise effects in the nonlinear thermoelectricity of a Josephson junction, *Appl. Phys. Lett.* **117**, 212601 (2020).
- [30] G. Germanese, F. Paolucci, G. Marchegiani, A. Braggio, and F. Giazotto, Bipolar thermoelectric Josephson engine, *Nat. Nanotechnol.* **17**, 1084 (2022).
- [31] G. Germanese, F. Paolucci, G. Marchegiani, A. Braggio, and F. Giazotto, Phase Control of Bipolar Thermoelectricity in Josephson Tunnel Junctions, *Phys. Rev. Appl.* **19**, 014074 (2023).
- [32] F. Giazotto, F. Paolucci, A. Braggio, G. Marchegiani, and G. Germanese, Superconducting bipolar thermoelectric memory and method for writing a superconducting bipolar thermoelectric memory, Patent (21/12/2021), filing number: 102021000032042.
- [33] G. Germanese, F. Paolucci, G. Marchegiani, A. Braggio, and F. Giazotto, Spontaneous symmetry breaking induced thermospin effect in superconducting tunnel junctions, *Phys. Rev. B* **104**, 184502 (2021).
- [34] C. Guarcello, A. Braggio, P. Solinas, and F. Giazotto, Nonlinear Critical-Current Thermal Response of an Asymmetric Josephson Tunnel Junction, *Phys. Rev. Appl.* **11**, 024002 (2019).
- [35] C. Guarcello, R. Citro, F. Giazotto, and A. Braggio, Temperature-Biased Double-Loop Josephson Flux Transducer, *Phys. Rev. Appl.* **18**, 014037 (2022).
- [36] C. Kittel, *Introduction to Solid State Physics* (John Wiley & sons, Inc. (New York), 1986), 6th ed.
- [37] M. Tinkham, *Introduction to Superconductivity* (McGraw-Hill, New York, 1996), 2nd ed.
- [38] L. Bernazzani, *Nonlinear Thermoelectricity in Nano-Devices*, Master's thesis, University of Pisa (2021).
- [39] J. B. Oostinga, H. B. Heersche, X. Liu, A. F. Morpurgo, and L. M. K. Vandersypen, Gate-induced insulating state in bilayer graphene devices, *Nat. Mater.* **7**, 151 (2008).
- [40] Y. Zhang, T. Tang, C. Girit, Z. Hao, M. Martin, A. Zettl, M. Crommie, Y. R. Shen, and F. Wang, Direct observation of a widely tunable bandgap in bilayer graphene, *Nature* **459**, 820 (2009).
- [41] E. V. Castro, K. S. Novoselov, S. V. Morozov, N. M. R. Peres, J. M. B. L. dos Santos, J. Nilsson, F. Guinea, A. K. Geim, and A. H. Castro Neto, Electronic properties of a biased graphene bilayer, *J. Phys. Condens. Matter* **22**, 175503 (2010).
- [42] E. McCann and M. Koshino, The electronic properties of bilayer graphene, *Rep. Prog. Phys.* **76**, 056503 (2013).
- [43] The lowest-energy bands shown in the plot are obtained using Eq. (43) of Ref. [42] and relating the potential, U , to the band gap, $2E_g$, with Eq. (1).
- [44] A. Balandin, Thermal properties of graphene and nanostructured carbon materials, *Nat. Mater.* **10**, 569 (2011).

- [45] M. S. Dresselhaus, G. Dresselhaus, X. Sun, Z. Zhang, S. B. Cronin, and T. Koga, Low-dimensional thermoelectric materials, *Phys. Solid State* **41**, 679 (1999).
- [46] K. Novoselov, A. Geim, S. Morozov, D. Jiang, M. Katsnelson, I. V. Grigorieva, S. V. Dubonos, and A. A. Firsov, Two-dimensional gas of massless Dirac fermions in graphene, *Nature* **438**, 197 (2005).
- [47] M. Sprinkle, D. Siegel, Y. Hu, J. Hicks, A. Tejada, A. Taleb-Ibrahimi, P. Le Fèvre, F. Bertran, S. Vizzini, H. Enriquez, S. Chiang, P. Soukiassian, C. Berger, W. A. de Heer, A. Lanzara, and E. H. Conrad, First Direct Observation of a Nearly Ideal Graphene Band Structure, *Phys. Rev. Lett.* **103**, 226803 (2009).
- [48] E. McCann, Asymmetry gap in the electronic band structure of bilayer graphene, *Phys. Rev. B* **74**, 161403 (2006).
- [49] J. Sławińska, I. Zasada, and Z. Klusek, Energy gap tuning in graphene on hexagonal boron nitride bilayer system, *Phys. Rev. B* **81**, 155433 (2010).
- [50] K. F. Mak, C. H. Lui, J. Shan, and T. F. Heinz, Observation of an Electric-Field-Induced Band Gap in Bilayer Graphene by Infrared Spectroscopy, *Phys. Rev. Lett.* **102**, 256405 (2009).
- [51] F. Vischi, M. Carrega, A. Braggio, F. Paolucci, F. Bianco, S. Roddaro, and F. Giazotto, Electron Cooling with Graphene-Insulator-Superconductor Tunnel Junctions for Applications in Fast Bolometry, *Phys. Rev. Appl.* **13**, 054006 (2020).
- [52] J. K. Viljas and T. T. Heikkilä, Electron-phonon heat transfer in monolayer and bilayer graphene, *Phys. Rev. B* **81**, 245404 (2010).
- [53] The top and bottom gates are referenced to the BLG ohmic contacts to induce a proper gating on the BLG, which is not affected by the bias applied to the junction.
- [54] C. Maestre, B. Toury, P. Steyer, V. Garnier, and C. Journet, Hexagonal boron nitride: A review on selfstanding crystals synthesis towards 2D nanosheets, *J. Phys. Mater.* **4**, 044018 (2021).
- [55] M. Tinkham, Tunneling generation, relaxation, and tunneling detection of hole-electron imbalance in superconductors, *Phys. Rev. B* **6**, 1747 (1972).
- [56] J. B. Ketterson and S. N. Song, *Superconductivity* (Cambridge University Press, Cambridge, 1999).
- [57] F. Giazotto, T. T. Heikkilä, A. Luukanen, A. Savin, and J. P. Pekola, Opportunities for mesoscopics in thermometry and refrigeration: Physics and applications, *Rev. Mod. Phys.* **78**, 217 (2006).
- [58] R. C. Dynes, J. P. Garno, G. B. Hertel, and T. P. Orlando, Tunneling Study of Superconductivity near the Metal-Insulator Transition, *Phys. Rev. Lett.* **53**, 2437 (1984).
- [59] E. Suárez Morell and L. E. F. Foa Torres, Radiation effects on the electronic properties of bilayer graphene, *Phys. Rev. B* **86**, 125449 (2012).
- [60] *h*-BN is commonly used to encapsulate graphene, since its crystalline configuration matches well with that of graphene, diminishing surface disorder at the interfaces.
- [61] The conductance, $G_T = 4N_F e^2 |T|^2 t_{\perp} / (\hbar \sqrt{3} t^2)$, would represent the differential conductance of the tunnel junction when the superconductor is in the normal state and the BLG is gapless.
- [62] L. Britnell, R. V. Gorbachev, R. Jalil, B. D. Belle, F. Schedin, M. I. Katsnelson, L. Eaves, S. V. Morozov, A. S. Mayorov, N. M. R. Peres, A. H. Castro Neto, J. Leist, A. K. Geim, L. A. Ponomarenko, and K. S. Novoselov, Electron tunneling through ultrathin boron nitride crystalline barriers, *Nano Lett.* **12**, 1707 (2012).
- [63] M. Ramezani, I. Sampaio, K. Watanabe, T. Taniguchi, C. Schönenberger, and A. Baumgartner, Superconducting contacts to a monolayer semiconductor, *Nano Lett.* **21**, 5614 (2021).
- [64] J. E. Padilha, R. B. Pontes, and A. Fazzio, Bilayer graphene on *h*-BN substrate: Investigating the breakdown voltage and tuning the bandgap by electric field, *J. Phys. Condens. Matter* **24**, 075301 (2012).
- [65] A. H. Castro Neto, F. Guinea, N. M. R. Peres, K. S. Novoselov, and A. K. Geim, The electronic properties of graphene, *Rev. Mod. Phys.* **81**, 109 (2009).
- [66] Y. Dubi and M. Di Ventra, Colloquium: Heat flow and thermoelectricity in atomic and molecular junctions, *Rev. Mod. Phys.* **83**, 131 (2011).
- [67] In principle, by inverting the ratio between E_g and $\Delta_{0,R}$, the opposite temperature gradient may be assumed, but this is less practical, since the temperature of the superconducting lead should not exceed its critical temperature in any case.
- [68] S. Kheradsoud, N. Dashti, M. Misiorny, P. P. Potts, J. Splettstoesser, and P. Samuelsson, Power, efficiency and fluctuations in a quantum point contact as steady-state thermoelectric heat engine, *Entropy* **21**, 777 (2019).
- [69] Even if the absolute value of these quantities also depends on the Dynes parameter, Γ_D , the general behavior will be quite independent of it.
- [70] Obviously, heat may potentially be transferred by other contributions, such as phonon or even radiative contributions, that are more difficult to estimate. Our computation of efficiency represents a sort of optimal electronic efficiency of the device.
- [71] G. Alymov, V. Vyurkov, V. Ryzhii, and D. Svintsov, Abrupt current switching in graphene bilayer tunnel transistors enabled by van Hove singularities, *Sci. Rep.* **6**, 24654 (2016).
- [72] E. Icking, L. Banszerus, F. Wörtche, F. Volmer, P. Schmidt, C. Steiner, S. Engels, J. Hesselmann, M. Goldsche, K. Watanabe, T. Taniguchi, C. Volk, B. Beschoten, and C. Stampfer, Transport spectroscopy of ultraclean tunable band gaps in bilayer graphene, *Adv. Electron. Mater.* **8**, 2200510 (2022).
- [73] The presence of localized charge states induced by impurities also determines a modification of the gating conditions, but these contributions can be simply accounted for by including appropriate offsets to the gate voltages, so we neglect them [72].
- [74] The band-gap self-consistent expression of Eq. (6) is derived using Eqs. (65) and (74) of Ref. [42] in the limit with $\epsilon_r \sim 1$, $\Lambda \sim 1$, and assuming no mobile charge density when the Fermi energy is in the gap. Correspondingly, the Fermi-energy expression, Eq. (7), coincides with the chemical potential of Eq. (S13) of the Supplemental Material of Ref. [72], which neglects terms involving the inverse of BLG capacitance, C_{BLG}^{-1} , where $C_{\text{BLG}} \gg C_b, C_t$.

- [75] This simplified model may not be fully self-consistent when the system is gated well outside the gap, but corrections are expected to slightly renormalize the gap value without affecting the physics discussed.
- [76] F. Paolucci, G. Germanese, A. Braggio, and F. Giazotto, A highly-sensitive broadband superconducting thermoelectric single-photon detector, (2023), arXiv preprint [ArXiv:2302.02933](https://arxiv.org/abs/2302.02933).
- [77] F. Xia, T. Mueller, Y. Lin, A. Valdes-Garcia, and P. Avouris, Ultrafast graphene photodetector, *Nat. Nanotech.* **4**, 839 (2009).
- [78] T. Mueller, F. Xia, and P. Avouris, Graphene photodetectors for high-speed optical communications, *Nat. Photon.* **4**, 297 (2010).
- [79] G. H. Lee, D. K. Efetov, W. Jung, L. Ranzani, E. D. Walsh, T. A. Okhi, T. Taniguchi, K. Watanabe, P. K. D. Englund, and K. C. Fong, Graphene-based Josephson junction microwave bolometer, *Nature* **586**, 42 (2020).
- [80] A. Varpula, A. V. Timofeev, A. Shechetov, K. Grigoras, J. Hassel, J. Ahopelto, M. Ylilammi, and M. Prunnila, Thermoelectric thermal detectors based on ultra-thin heavily doped single-crystal silicon membranes, *Appl. Phys. Lett.* **110**, 262101 (2017).
- [81] T. T. Heikkilä, R. Ojajärvi, I. J. Maasilta, E. Strambini, F. Giazotto, and F. S. Bergeret, Thermoelectric Radiation Detector Based on Superconductor-Ferromagnet Systems, *Phys. Rev. Appl.* **10**, 034053 (2018).
- [82] Z. Geng, A. P. Helenius, T. T. Heikkilä, and I. J. Maasilta, Superconductor-ferromagnet tunnel junction thermoelectric bolometer and calorimeter with a SQUID readout, *J. Low Temp. Phys.* **199**, 585 (2020).
- [83] A. Varpula, K. Tappura, J. Tiira, K. Grigoras, O.-P. Kilpi, K. Sovanto, J. Ahopelto, and M. Prunnila, Nanothermoelectric infrared bolometers, *APL Photon.* **6**, 036111 (2021).